

## ARTICLE OPEN



# Proposing two-dimensional covalent organic frameworks material for the capture of phenol molecules from wastewaters

Afsaneh Ghahari<sup>1</sup>, Heidar Raissi<sup>1</sup> , Samaneh Pasban<sup>1</sup> and Farzaneh Farzad<sup>1</sup>

Industrial wastewater organic pollutants such as phenol can be treated through adsorption on active surfaces. Herein, the adsorption mechanism and dynamic behaviors of phenol molecules onto covalent organic frameworks (COFs) with well-defined supramolecular structures are investigated via molecular dynamics and well-tempered metadynamics simulations under various external electric fields. The Lennard–Jones interaction is predominant during the adsorption process, while NH and OH groups in COFs and phenol, respectively, can increase the adsorption due to the electrostatic interaction. Besides, the adsorption affinity of phenol on COFs is weakened by increasing the electric field strength. In addition, the free energy values for the complexes with and without the external electric field at their global minima reached at about  $-264.68$ ,  $-248.33$ , and  $-290.13$  (for 1, 0.5, and 0 V nm<sup>-1</sup>) kJ mol<sup>-1</sup>, respectively. The obtained results confirmed the COFs as prominent adsorbents for loading phenol and its removal from the water-contaminated environment.

npj Clean Water (2022)5:28; <https://doi.org/10.1038/s41545-022-00173-2>

## INTRODUCTION

Phenol<sup>1</sup> (carbolic acid as IUPAC nomenclature) is the most common aromatic pollutant in several industrial wastewaters, including chemical industries<sup>2</sup> such as electroplating<sup>3</sup>, mining<sup>4</sup>, dyeing<sup>5</sup>, petrochemistry<sup>6</sup>, and so on<sup>7</sup>. This highly durable molecule has a high toxicity effect, especially on aquatic life, even at a low concentration. Among such adverse effects, phenol's harmful impact on the central nervous system is the most famous one, which leads to anorexia, insomnia, and various other detrimental subsequent<sup>8,9</sup>. Because of its toxicity, the removal of phenols<sup>10</sup> from industrial wastewater flow and just before their discharge into water reservoirs is thus obligatory. Otherwise, it will be led to a serious deterioration of usable water resources<sup>11,12</sup>. It is important to note that phenol removal from wastewaters is difficult because many different minerals salts such as sodium, cadmium, lead, calcium, and zinc coexist with phenol in this environment. Extraction of polar phenols in aqueous samples is challenging due to their hydrophobicity, very low concentration, and complexity. Therefore, the treatment of wastewaters containing resistant organic matters such as phenols has attracted much attention. For this purpose, many researchers have proposed several methods, such as adsorption, catalytic oxidation<sup>13</sup>, thermal oxidation<sup>14</sup>, condensation<sup>15</sup>, and ion exchange<sup>16</sup>. Among them, the adsorption process is considered one of the most influential, and economical methods for water cleansing<sup>17,18</sup>. One of the most efficient methods is to use porous solid substrates to adsorb and separate pollutants from the water.

Two-dimensional covalent organic frameworks (COFs) are an emerging class of highly ordered porous materials that can be fabricated in the 2D plane with many potential applications. It is worth mentioning that COFs are versatile materials and crystalline polymers with regular pores, which are widely used to adsorb contaminants due to their high porosity and modifiable skeleton<sup>19,20</sup>. In fact, COFs have attracted much attention as a platform because of their physicochemical properties<sup>21</sup>, nano-porous structure, mechanical robustness<sup>22</sup>, high design flexibility<sup>23</sup>, excellent solvent, thermal stabilities<sup>12</sup>, well-proportioned cavities<sup>24</sup>, low

densities<sup>25</sup>, and high specific surface areas<sup>26</sup>. Besides, these materials have strong interactions against loadings nanoparticles with high stability in acidic/aqueous/alkaline<sup>27–29</sup> mediums.

Recently, these materials have been synthesized as an extension of carbon porous materials with more than one kind of repeating unit (or monomer). Up to now, few studies have reported the capability of COFs and their derivatives as favorable nanostructures for wastewater remediation. Ever since the reported COFs structures by Côté et al.<sup>30</sup>, these compounds have constantly attracted the attention of medicinal and biochemical scientists<sup>31,32</sup>. The development of COFs-based materials with superior properties in separation science and technology is also of enormous interest. For instance, Zhang et al. used an ultra-stable sp<sup>2</sup> carbon-conjugated covalent organic framework (COFs-PDAN-AO) for efficient adsorption and detection of uranium from radioactive wastewater. Their result showed that COFs have high uranium adsorption capacity and can be potentially used for the removal of the uranium ions from the radioactive wastewaters. Also, they found that COFs-PDAN-AO well maintained structural stability and may be used for the extraction of other contaminants too<sup>33</sup>. Shang et al. reported the adsorption mechanisms of three types of nanoplastics, including polyethylene terephthalate, polyethylene, and nylon-6 on the COF (TpPa-X, X = CH<sub>3</sub>, H, NO<sub>2</sub>, OH, and F) via the molecular dynamic (MD) simulations. They found that TpPa-OH has the strongest adsorption sites for the nanoplastics pollutants. In addition, their results reveal that the COF-polymer at the atomic scale can be used for the development of promising COF materials to deal with NP pollution<sup>34</sup>. More recently, Li et al. synthesized superhydrophobic sponges (sponges@COFs) components at room temperature. Furthermore, the practical application of the sponges@COFs was also evaluated for the removal of oil suspension from industrial wastewater. The results showed that the sponges@COFs have the ultra-high adsorption capacity for various organic solvents and oil and also could effectively remove oil from water and achieve rapid oil-water separation<sup>35</sup>. Chen et al. explored the self-standing 2D sulfonate anionic COF membrane and found that it could be used

<sup>1</sup>Department of Chemistry, University of Birjand, Birjand, Iran. ✉email: hraeisi@birjand.ac.ir

as an absorbent for the removal of cationic organic contaminants from the environment. They also showed that the COF membrane maintains a rigid porous structure through high porosity that can be employed for nanofiltration and organic pollutants separation applications<sup>36</sup>.

Besides, three-dimensional COFs with a diamond topology, as a porous platform, synthesized by Wang et al., are used for the removal of radioactive vapor wastes in the fission process. It was found that three-dimensional COFs enable the removal of iodine vapor through the formation of charge–transfer complex with the pore’s walls<sup>37</sup>. Wang et al. also investigated the class of cationic COF, which is synthesized via an imine condensation reaction, for efficient removal of hexafluoropropylene oxide trimer acid (HFPO-TA) and hexafluoropropylene oxide dimer acid (GenX), as environmental contaminants from aqueous solution. The results revealed that cationic COFs with quaternary ammonium have a high adsorption capacity for HFPO-TA (2.16 mmol g<sup>-1</sup>) and GenX (2.06 mmol g<sup>-1</sup>), which are more efficient than carbon and conventional activated resins<sup>38</sup>.

This work focuses on a biocompatible nanoparticle platform, namely, the self-assembled COFs structure, and how this nanostructure can be used as distinguished adsorbents to remove dangerous phenol pollutants from the environment in the presence of an electrical field. Therefore, in this study, via classical MD simulation, we studied the interfacial adsorption mechanisms of phenol pollutants on well-established COFs, which show advantages in environmental friendliness. Depending on the molecular structure of COFs with the presence of different electric fields, two interactions such as electrostatic interaction and van der Waals (vdW) interaction are identified to be responsible for the adsorption of phenol pollutants on COFs. Furthermore, to determine the penetration of phenol on the COFs nanostructure, a series of parameters such as the number of hydrogen bonding, radius distribution function, and the diffusion coefficient of phenol for three simulated systems are analyzed. First, a discussion about the self-assembled COFs nanostructure that can act as the adsorbent for removing pollution in the absence of an electric field is provided. Next, the ability of this nanostructure to exclude the pollutant by imposing an external electric field supplied a basis for understanding how the EF will affect the pollutant adsorption. It is found that when interacting phenol with COFs, while the EF = 0, the adsorption energy is the highest while EF = 1 shows the lowest adsorption energy value. The well-tempered metadynamics simulations are performed for each system under zero-field conditions and then via an imposing an external electric field to obtain free energy profiles. The obtained results confirm the high potential of COFs as the porous material for the solvation of the world’s threatening pollution issues. Therefore, the capability to remove dangerous phenol pollutants from the environment can be enhanced through the predesigning of the molecular structure, which provides a strong basis for the practical application of COFs as a potential adsorbent. In summary, our objective in the present study is to answer the following questions: (1) under what conditions do these phenol molecules are removed from the environment? (2) How does the electric field affect the adsorption of phenol molecules on the COFs nanostructure? (3) Can the COFs nanostructure be applied as the removal pollutant system for industrial wastewater treatment?

## RESULT AND DISCUSSION

### MD simulation

According to the modeled substrate, the thickness of COF is about 10 Å. Therefore, the adsorption area is divided into the internal part (<10 Å) and the outside part (>10 Å) of the COFs. The structures of COFs nano-channels and phenol molecules are presented in Supplementary Fig. 1. Our simulations can be divided into three setups (see Table 1): (a) COFs/phenol without EF; (b) COFs/phenol under an applied EF of 0.5 V nm<sup>-1</sup>; (c) COFs/phenol with a presence of EF of 1 V nm<sup>-1</sup>. Snapshots of MD simulations, which are presented in Fig. 1, show the final (105 ns) states of the studied systems. It can be seen that at EF = 0 and 0.5, the phenol molecules are not only adsorbed on the substrate surface but also, more importantly, can effectively infiltrate into the COFs, and also, form stronger interactions with the atoms of the COFs nano-channels. On the other hand, under the influence of an electric field at 1 V nm<sup>-1</sup>, the adsorbate molecules practically cannot enter into the cavities’ COFs, and they overlap together.

These preconceptions will be estimated via many informative analyses as follow. The interaction energies between phenol molecules and the substrate are averaged and provided in Table 2. Besides, the averaged interaction energies for the last five ns of each simulation system are also presented in Fig. 2. From the viewpoint of the composition of the interaction energies, there’s no doubt that both  $E_{vdw}$  and  $E_{elec}$  play a substantial role both  $E_{vdw}$  and  $E_{elec}$  play the main role in the adsorption process, and also seen with the increase of the electric field strengths, the interactions decrease (Fig. 2). As shown in Table 2, the value of the COFs–phenol (C–P) interaction energy decreases in the presence of the external electrical field. At the same time, this reduction is more significant for the electrical field of 1 V nm<sup>-1</sup>. This behavior is probably due to the formation of  $\pi$ – $\pi$  stacking interactions between the benzene ring of phenol molecules that increase the molecule rigidity and hinders their movement. In contrast, under zero and 0.5 V nm<sup>-1</sup> of EF, the adsorbate molecules can penetrate into the channels of COFs, and its OH functional group extensively interacts with N atoms of the substrate; therefore, interaction energies considerably increase.

These results can be better presented through calculations relating to the mean squared displacement. Diffusion coefficient ( $D_i$ ) acts as a quantitatively significant descriptor of MD and can provide information about molecular diffusion. In this paper, the diffusion coefficient is calculated using the “Einstein” relation<sup>39</sup>.

$$D = \lim_{t \rightarrow \infty} 1/6t[r_i(t) - r_i(0)]^2 \quad (1)$$

The calculated self-diffusion coefficient ( $D_p$ ) for phenol molecules under different strengths of external electric fields of 0, 0.5, and 1.0 V nm<sup>-1</sup> is 0.1172, 0.0715, and 0.0155 (1e–5 cm<sup>2</sup> s<sup>-1</sup>), respectively (see Supplementary Fig. 2). As it is obvious from Supplementary Fig. 2, imposing the external electric field caused the  $D_i$  of phenol decrease. Indeed, the diffusion of adsorbate molecules on the surface and inside channels of COFs decreases with increasing the electrical field intensity. This phenomenon can be attributed to the strong hydrogen bond (HB) between the phenol hydroxyl group and water molecules in the presence of the strongest field, in result shielding the interactions between adsorbate and the carrier. These features can lead to the self-diffusivity and random

**Table 1.** Details of the simulation pattern.

Systems	No. phenol	No. water	Box size (nm <sup>3</sup> )	No. Na	No. Cl
COF–Phenol–EF 0	50	4664	4 × 4 × 10	14	44
COF–Phenol–EF 1	50	4664	4 × 4 × 10	14	44
COF–Phenol–EF 0.5	50	4664	4 × 4 × 10	14	44

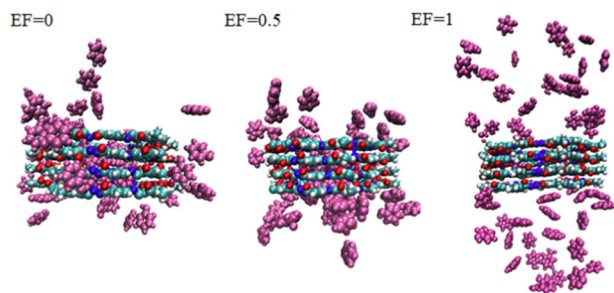


**Fig. 1** The final snapshots of the phenol-COFs complexes under different electrical fields. Water molecules and ions are not shown for clarity.

**Table 2.** The electrostatic (Elec), van der Waals (vdW), and total energies (in  $\text{kJ mol}^{-1}$ ) between the phenol molecules and the COFs nano-channel in various systems.

System	Total	van der Waals	Elec
COF-Phenol-EF 0	-396.047	-215.391	-180.656
COF-Phenol-EF 1	-86.125	-37.569	-48.556
COF-Phenol-EF 0.5	-328.357	-176	-152.357

reorientation of phenol molecules within the solvent medium (low  $D_i$  value).

In addition, the molecular interactions can be examined via the radial distribution functions (RDF) of adsorbate molecules at a distance  $r$  from the adsorbent slabs<sup>40</sup>. RDF ( $g(r)$ ) is calculated as the following equation:

$$g(r) = \frac{n(r)}{2\pi r \Delta r \rho} \quad (2)$$

where  $r$  (nm) is the given distance from the atoms of the substrate,  $n(r)$  is the time-averaged number of adsorbate molecules in the area of  $r \pm \Delta r$ , and  $\rho$  is the density of the system.

To explore the nature of interactions between the phenol molecules and the COFs substrates, the RDF patterns between C-P and phenol-water (p-w) are calculated, and obtained results are presented in Fig. 3. As seen in this figure, the application of the external electric fields reduced the maximum height of the RDF peaks. In addition, as can be seen in the RDF pattern, this decrease is much more for  $EF = 1$ , where the exact position of the peak cannot be distinguished. In fact, when the electric field strength equals  $1.0 \text{ V nm}^{-1}$ , no significant adsorption has happened. Instead, it shows an obvious downward trend; therefore, the probability of finding phenol molecules in short distances is close to zero due to observed strong repulsion forces between the adsorbate molecules and the substrate.

Interestingly, many other studies reported the same results and confirmed that the external electric field could effectively weaken such interactions. For example, Jiao et al. explored the interactions of phenol molecules with graphene oxide<sup>41</sup> surface. They detected a hindering impact on the adsorption process as the external electrical fields were implemented. Han et al. also showed a weakening in the interactions as the electric field is imposed. Besides, the strongest RDF peak at  $EF = 0$  is located at  $\sim 0.5 \text{ nm}$ . This result may be related to the comparatively strong interaction between H atoms of the hydroxyl group in phenol and N atoms in COFs nano-channel and the  $\pi$ - $\pi$  hydrophobic interactions between the aromatic rings of existing compounds.

These findings are confirmed by the final snapshots of the adsorption structures (Fig. 1), where the obtained configuration is consistent with the RDF curves. As evident in Fig. 3, the position of the observed peak in the  $g_{p-w}(r)$  curves posed at  $0.36 \text{ nm}$ , and this

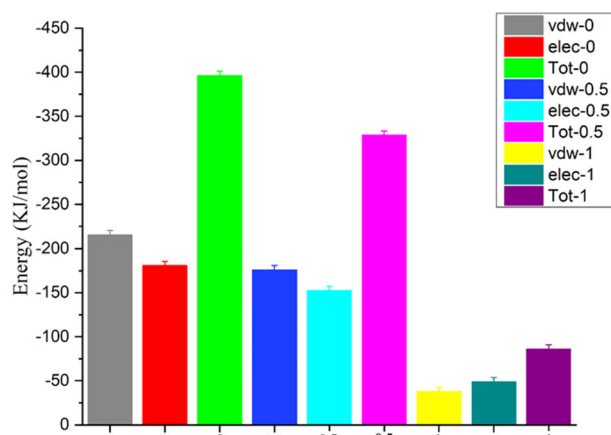


**Fig. 2** The interaction energy between phenol molecules and COFs under an electrical field with different strengths and zero field. The error bars represent the standard deviations of the data.

position does not affect by the implementation of the various magnitude of EF. A comparison of the  $g_{p-w}(r)$  curves revealed that the presence of EF can increase the p-w interaction and can lead to higher distribution probabilities for water molecules around phenol, which obviously prevent the interactions between the phenol molecule and the substrate.

The formation of HBs plays an essential role in the exploration of the stability of the resulting complex. Moreover, the extent of electrostatic interactions is usually reflected in the number of HBs, too. The identification and analysis of the H-bonding are based on the calculation of pairwise interactions between donor and acceptor atoms at less than  $3.5 \text{ \AA}$  distance and an angle cutoff of  $30^\circ$ . Therefore, the number of HBs of phenol/COFs and phenol/water are computed at any time step of the simulation. The obtained HBs diagrams in systems with various EF are presented in Fig. 4a, b, wherein it can be seen that there are significant variations in the numbers of HBs formed under the various strength of EFs. Moreover, the number of HBs between the COFs rings and phenol molecules is remarkably reduced under electric fields strength of  $0.5$  and  $1.0 \text{ V nm}^{-1}$ . In contrast, the number of H-bonds shows a monotonous increasing trend in the external EF of zero (see in Fig. 4a).

Precisely speaking, when there is no external electric field, the phenol molecules stay close to the COFs surface due to the HBs interactions between the amine and hydroxyl groups of the COFs surface and hydroxyl groups of phenol molecules. Moreover, -OH functional groups of phenols are proved to play an essential role in forming HBs. Also, the number of HBs formed by multiple  $\text{O}-\text{H}\cdots\text{O}$  pairs of the coordinated water donors and the acceptor hydroxyl group of phenols are investigated under the external electric field with different strengths (Fig. 4b). Our results illustrate that an enhancement in the number of H-bonds between the phenol molecules and the COFs surface is dependent on a reduction in the number of H-bonds between the water and phenol molecules. It is essential to the reminder that there are plenty of other articles that applied MD simulations for the study of similar systems and their results are in good agreement with our data<sup>41-43</sup>.

### Metadynamics

The well-tempered metadynamics simulation is a method that allows the acceleration of the rare events and the estimation of the free energy surface (FES) to describe complex molecular systems<sup>44</sup>. The metadynamics technique is used to calculate the FES as a function of distances between the center of masses (COMs) of two components based on methods proposed by Parrinello and Laio.

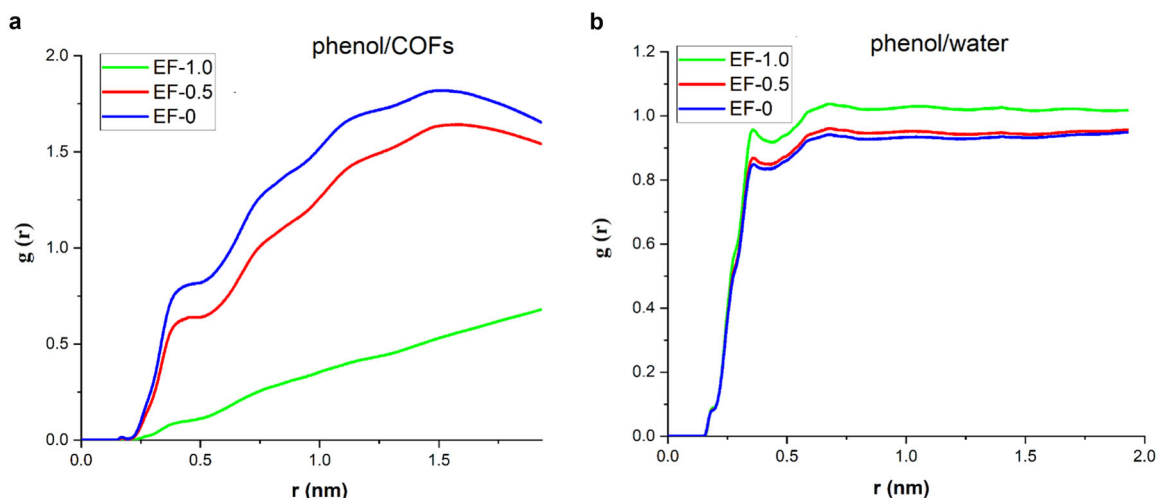


**Fig. 3** RDF patterns. **a** Between phenol and COFs. **b** Between phenol and water.

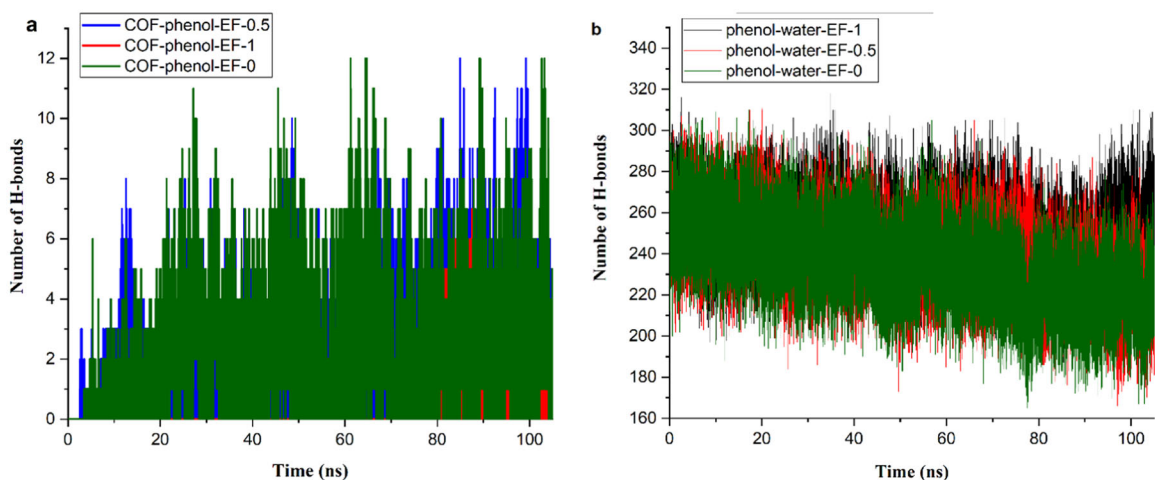


**Fig. 4** The number of hydrogen bonds against the simulation time. **a** Between COF and phenol. **b** Between phenol and water.

Metadynamics simulations are carried out for 105 ns for all investigated systems. We utilized these simulations to study the dissociation and association events and the free-energy landscape of the C–P complexes. It is worth mentioning that the simulation was performed multiple times in the presence of the different external EFs at 1, 0.5, and 0  $\text{V nm}^{-1}$ . Our obtained results confirm that the electric field can be used to trigger the controlled release of the phenol molecules from the COFs structure.

Obtained FES patterns as a function of the distance between the COM of the phenol molecule and COFs are depicted in Figs. 5–7. Free energy is set to zero for long distances between COMs of COFs and the phenol molecule. It is worth mentioning that, in free energy calculations, the COM of COFs is selected as a corrective variable, and collective variable (CV) =  $-6$  is related to the left-hand part of COFs monolayers.

The FES pattern in Fig. 7 represents the phenol and carrier complex in the presence of an EF with the strength of 0  $\text{V nm}^{-1}$  that has the highest free energy in its steady-state. The free energy values of C–P complexes in the presence of the electric fields equal to 1, 0.5, and 0  $\text{V nm}^{-1}$  at their global minimums are

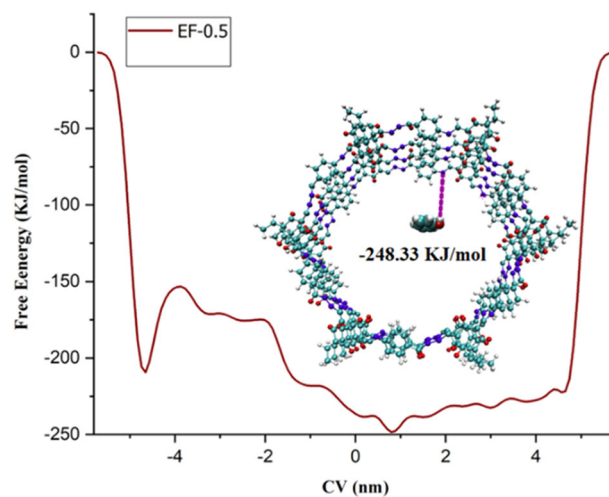


**Fig. 5** The free energy profile with imposing an electrical field at 0.5  $\text{V nm}^{-1}$ . Water molecules are not shown for clarity.



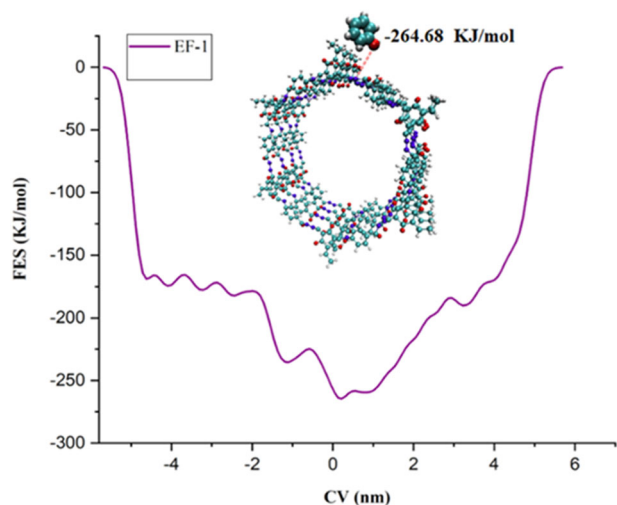


**Fig. 6** The free energy profile with imposing an electrical field at  $1 \text{ V nm}^{-1}$  condition.

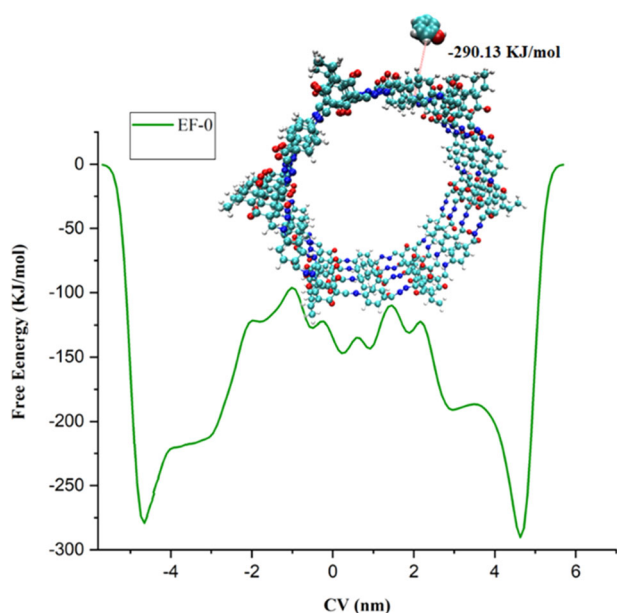


**Fig. 7** The free energy profile under zero electrical field condition.

about  $-264.68$ ,  $-248.33$ , and  $-290.13 \text{ kJ mol}^{-1}$ , respectively. A decrease in the value of the free energy between phenol molecule and COFs structure is observed by the increase of field strength up to  $0.5$  and  $1.0 \text{ V nm}^{-1}$ , Figs. 5 and 6. This finding is also in agreement with interaction energies in Table 2, where the values become less negative, and interactions are a bit repulsive. The decrease of the free energy values in the investigated systems indicates that the EF acts as a motive force on the phenol release from the nanocarrier.

In addition, the overall result, the COF nanocarrier is a good candidate for adsorption of phenol molecules, as well; the evaluation of the dynamic behavior in response to the application of an external EF with different strengths shows that the implemented EFs act as a motive force in the release of the phenol molecule from the nanostructure.

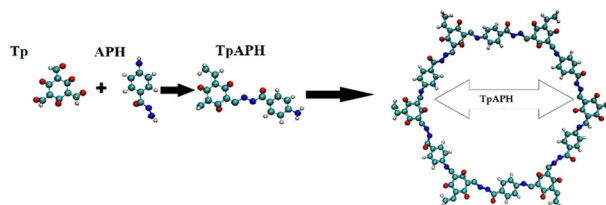


**Fig. 8** Schematic representation of the formation of COF. Color code: C, cyan; O, red; N, blue; H, white.

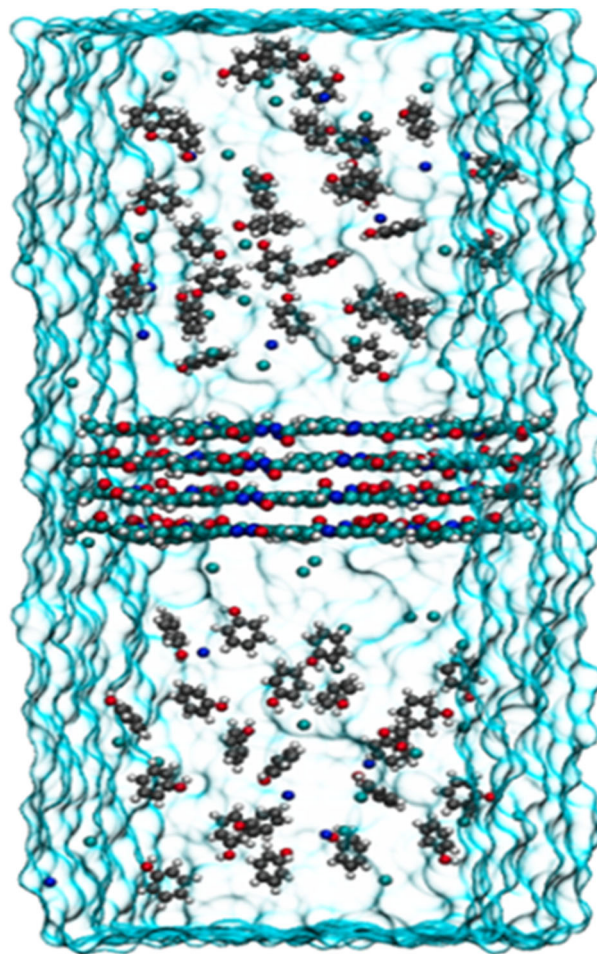


**Fig. 9** The initial snapshot of the studied systems. Color code COFs: cyan, phenol: gray, ions: green, and blue.

## METHODS

### MD simulations

The MD simulation is applied to investigate the potential of COF carrier as a promising candidate for the remediation of phenol-contaminated wastewater. The initial geometry of the COFs carrier is taken from our previous work<sup>45</sup>, which is inspired by Mitra et al.'s work<sup>46</sup>.

The non-hydroxyl COFs nanostructure contains the linker units of TpAPH monomers. It is noteworthy to mention that the TpAPH monomer is synthesized via salt-mediated Schiff 1,3,5-triformylphloroglucinol (Tp) and 4-aminobenzohydrazide (APH). Such COFs pores have a vdW diameter of  $27.08 \text{ \AA}$  and are created based on the strong covalent interactions. The schematic representation of the COF and its monomer is shown in Fig. 8. The COFs structure is designed in four layers, including 776 atoms, which is made by using the GaussView software<sup>47</sup>. Here, the MD simulations are carried out using the software package GROMACS (version 2019.2)<sup>48</sup> with CHARMM 36 force field<sup>49</sup>. A simulation box with

the dimension of  $4 \times 4 \times 10 \text{ nm}^3$ , containing a COFs nanocarrier at the center and 50 phenol molecules, dissolved in 3795 TIP3P water model<sup>50</sup> with the salinity of 0.15 M NaCl, mimicking the correct physiological environment. The periodic boundary condition is also considered to prevent the interaction of components with their neighbor cells. The particle mesh Ewald method treats non-bonded electrostatic and Lenard–Jones interactions with a 1.4 nm cutoff. The temperature and pressure are maintained at 310 K, and 1 bar by using the Nose-hoover thermostat<sup>51</sup> and Parrinello–Rahman barostat<sup>52</sup>, respectively. The linear constraint solver algorithm<sup>53</sup> is employed to constrain all the bonds in the simulation at their equilibrium length. At first, to reduce any unfavorable interactions, the simulation system is relaxed via energy minimization by using the steepest descent algorithm<sup>54</sup>. Finally, MD simulations are performed for 105 ns with a time step of 1.5 fs. The initial snapshot of the studied systems is shown in Fig. 9. The visual MD package is utilized for visualizing the simulated products<sup>55</sup>. It is worthy of mentioning that, in this study, to consider the impact of electrical field strength on the adsorption of phenol by COFs the external electric fields with different strengths are applied in the systems.

### Metadynamics simulations

Well-tempered metadynamics simulation is explored to detect the FES as a function of the set of CVs developed by Parrinello et al.<sup>56</sup>. The metadynamics simulations are performed by PLUMED plug-in version 2.5.2<sup>57</sup> implemented in Gromacs 2018 package<sup>58</sup>. In the well-tempered metadynamics algorithm the initial Gaussian height is  $1.0 \text{ kJ mol}^{-1}$ , and also the width is set to  $0.25 \text{ \AA}$ , respectively, with a bias factor of 15, which is deposited every 500 timesteps. It is worth noting that the metadynamics simulations are applied for 105 ns for all investigated systems. Generally, the metadynamics simulations depicted in this study provide a trustworthy approximation of the free energy landscape of COFs/phenol systems.

### DATA AVAILABILITY

The authors confirm that all relevant data are included in the article and/or its Supplementary information files.

Received: 6 February 2022; Accepted: 22 June 2022;

Published online: 07 July 2022

### REFERENCES

- Zhang, Q. et al. Molecular dynamics simulation of phenol aqueous solution under the impact of an external electrostatic field. *J. Chem. Eng. Data* **64**, 2259–2265 (2019).
- Luo, D. et al. How phenol stresses anammox for the treatment of ammonia-rich wastewater: phenomena, microbial community evolution and molecular modeling. *Bioresour Technol.* **347**, 126747 (2022).
- Ahmed, M. et al. Recent developments in hazardous pollutants removal from wastewater and water reuse within a circular economy. *npj Clean. Water* **5**, 1–25 (2022).
- Zhang, Y. et al. Ion exchange membrane optimized light-driven photoelectrochemical unit for efficiency simultaneous organic degradation and metal recovery from the mine wastewater. *J. Hazard. Mater.* **429**, 128352 (2022).
- Panimalar, S. et al. Reproducibility and long-term stability of Sn doped MnO<sub>2</sub> nanostructures: practical photocatalytic systems and wastewater treatment applications. *Chemosphere* **293**, 133646 (2022).
- Jothinathan, L., Cai, Q. Q., Ong, S. L. & Hu, J. Y. Fe-Mn doped powdered activated carbon pellet as ozone catalyst for cost-effective phenolic wastewater treatment: Mechanism studies and phenol by-products elimination. *J. Hazard. Mater.* **424**, 127483 (2022).
- Akçay, M. & Akçay, G. The removal of phenolic compounds from aqueous solutions by organophilic bentonite. *J. Hazard. Mater.* **113**, 189–193 (2004).
- Han, Y., Wang, N., Guo, X., Jiao, T. & Ding, H. Influence of ultrasound on the adsorption of single-walled carbon nanotubes to phenol: a study by molecular dynamics simulation and experiment. *Chem. Eng. J.* **427**, 131819 (2022).
- Mahnashi, M. H. et al. HPLC-DAD phenolics analysis,  $\alpha$ -glucosidase,  $\alpha$ -amylase inhibitory, molecular docking and nutritional profiles of *Persicaria hydropiper* L. *BMC Complement. Med. Ther.* **22**, 1–20 (2022).
- Abu-Nada, A., Abdala, A. & McKay, G. Removal of phenols and dyes from aqueous solutions using graphene and graphene composite adsorption: a review. *J. Environ. Chem. Eng.* **9**, 105858 (2021).
- Song, Z., Xiu, F.-R. & Qi, Y. Degradation and partial oxidation of waste plastic express packaging bags in supercritical water: resources transformation and pollutants removal. *J. Hazard. Mater.* **423**, 127018 (2022).
- Qi, X. et al. Recent advances in polysaccharide-based adsorbents for wastewater treatment. *J. Clean. Prod.* **315**, 128221 (2021).
- Ruan, Y. et al. Review on the synthesis and activity of iron-based catalyst in catalytic oxidation of refractory organic pollutants in wastewater. *J. Clean. Prod.* **321**, 128924 (2021).
- Chaghaganoj, Z. D., Asasian-Kolur, N., Sharifan, S. & Sillanpää, M. Ce and mn/bio-waste-based activated carbon composite: characterization, phenol adsorption and regeneration. *J. Environ. Chem. Eng.* **9**, 105788 (2021).
- Shi, Z. et al. Enhanced ferrate oxidation of organic pollutants in the presence of Cu (II) Ion. *J. Hazard. Mater.* **433**, 128772 (2022).
- Liu, X. et al. Adsorption of ammonia nitrogen and phenol onto the lignite surface: an experimental and molecular dynamics simulation study. *J. Hazard. Mater.* **416**, 125966 (2021).
- Hou, Y. et al. Metagenomics-based interpretation of the impacts of silica nanoparticles exposure on phenol treatment performance in sequencing batch reactor system. *Chem. Eng. J.* **428**, 132052 (2022).
- Nassar, H. N., El-Azab, W. I. M. & El-Gendy, N. S. Sustainable ecofriendly recruitment of bioethanol fermentation lignocellulosic spent waste biomass for the safe reuse and discharge of petroleum production produced water via biosorption and solid biofuel production. *J. Hazard. Mater.* **422**, 126845 (2022).
- Mellah, A. et al. Adsorption of pharmaceutical pollutants from water using covalent organic frameworks. *Chem. Eur. J.* **24**, 10601–10605 (2018).
- Karak, S. et al. Inducing disorder in order: hierarchically porous covalent organic framework nanostructures for rapid removal of persistent organic pollutants. *J. Am. Chem. Soc.* **141**, 7572–7581 (2019).
- Cui, Y. et al. Metal-organic frameworks as platforms for functional materials. *Acc. Chem. Res.* **49**, 483–493 (2016).
- Dey, K., Bhunia, S., Sasmal, H. S., Reddy, C. M. & Banerjee, R. Self-assembly-driven nanomechanics in porous covalent organic framework thin films. *J. Am. Chem. Soc.* **143**, 955–963 (2021).
- Kong, X., Zhou, S., Strømme, M. & Xu, C. Redox active covalent organic framework-based conductive nanofibers for flexible energy storage device. *Carbon N. Y.* **171**, 248–256 (2021).
- Choudhury, S. P. & Kalamdhad, A. S. Optimization of electrokinetic pretreatment for enhanced methane production and toxicity reduction from petroleum refinery sludge. *J. Environ. Manag.* **298**, 113469 (2021).
- Liu, R. et al. NaCl template-assisted synthesis of self-floating COFs foams for the efficient removal of sulfamerazine. *J. Hazard. Mater.* **421**, 126702 (2022).
- Chen, Y. et al. A silsesquioxane-porphyrin-based porous organic polymer as a highly efficient and recyclable adsorbent for wastewater treatment. *J. Hazard. Mater.* **406**, 124769 (2021).
- Bagheri, A. R., Aramesh, N., Sher, F. & Bilal, M. Covalent organic frameworks as robust materials for mitigation of environmental pollutants. *Chemosphere* **270**, 129523 (2021).
- Xia, Z., Zhao, Y. & Darling, S. B. Covalent organic frameworks for water treatment. *Adv. Mater. Interfaces* **8**, 2001507 (2021).
- Zheng, Q. et al. Single-crystalline covalent organic frameworks as high-performance liquid chromatographic stationary phases for positional isomer separation. *ACS Appl. Mater. Interfaces* **14**, 9754–9762 (2022).
- Côté, A. P. et al. Chemistry: porous, crystalline, covalent organic frameworks. *Science* **310**, 1166–1170 (2005).
- Li, K. et al. Postsynthetic modification of a covalent organic framework achieved via strain-promoted cycloaddition. *J. Am. Chem. Soc.* **143**, 649–656 (2021).
- Gao, P. et al. Covalent organic framework-derived carbonous nanopores for cancer cell imaging. *ACS Appl. Mater. Interfaces* **13**, 41498–41506 (2021).
- Li, F.-F. et al. Stable sp<sup>2</sup> carbon-conjugated covalent organic framework for detection and efficient adsorption of uranium from radioactive wastewater. *J. Hazard. Mater.* **392**, 122333 (2020).
- Shang, S. et al. Studying the adsorption mechanisms of nanoplastics on covalent organic frameworks via molecular dynamics simulations. *J. Hazard. Mater.* **421**, 126796 (2022).
- Li, J. et al. One-pot room-temperature synthesis of covalent organic framework-coated superhydrophobic sponges for highly efficient oil-water separation. *J. Hazard. Mater.* **411**, 125190 (2021).
- Chen, T. et al. Highly crystalline ionic covalent organic framework membrane for nanofiltration and charge-controlled organic pollutants removal. *Sep. Purif. Technol.* **256**, 117787 (2021).
- Wang, C. et al. A 3D covalent organic framework with exceptionally high iodine capture capability. *Chem. - A Eur. J.* **24**, 585–589 (2018).
- Wang, W. et al. Cationic covalent organic framework for efficient removal of PFOA substitutes from aqueous solution. *Chem. Eng. J.* **412**, 127509 (2021).

39. Liu, B., Goree, J. & Vaulina, O. S. Test of the Stokes-Einstein relation in a two-dimensional Yukawa liquid. *Phys. Rev. Lett.* **96**, 15005 (2006).
40. Kuntail, J., Jain, Y. M., Shukla, M. & Sinha, I. Adsorption mechanism of phenol, p-chlorophenol, and p-nitrophenol on magnetite surface: a molecular dynamics study. *J. Mol. Liq.* **288**, 111053 (2019).
41. Han, Y. et al. In-situ desorption of acetaminophen from the surface of graphene oxide driven by an electric field: a study by molecular dynamics simulation. *Chem. Eng. J.* **418**, 129391 (2021).
42. Han, Y., Zhang, Q. & Wu, L. Influence on the adsorption of phenol on single-walled carbon nanotubes caused by NaCl and an electrostatic field in saline. *Desalination* **477**, 114270 (2020).
43. Zhang, Q., Han, Y. & Wu, L. Influence of electrostatic field on the adsorption of phenol on single-walled carbon nanotubes: a study by molecular dynamics simulation. *Chem. Eng. J.* **363**, 278–284 (2019).
44. Laio, A. & Gervasio, F. L. Metadynamics: a method to simulate rare events and reconstruct the free energy in biophysics, chemistry and material science. *Rep. Prog. Phys.* **71**, 126601 (2008).
45. Ghahari, A., Raissi, H. & Farzad, F. Design of a new drug delivery platform based on surface functionalization 2D covalent organic frameworks. *J. Taiwan Inst. Chem. Eng.* **125**, 15–22 (2021).
46. Mitra, S. et al. Targeted drug delivery in covalent organic nanosheets (CONs) via sequential postsynthetic modification. *J. Am. Chem. Soc.* **139**, 4513–4520 (2017).
47. Dennington, R. et al. *GaussView, version 5*. (Wallingford, 2009).
48. Abraham, M. J. et al. Gromacs: high performance molecular simulations through multi-level parallelism from laptops to supercomputers. *SoftwareX* **1–2**, 19–25 (2015).
49. Huang, J. et al. CHARMM36m: an improved force field for folded and intrinsically disordered proteins. *Nat. Methods* **14**, 71–73 (2017).
50. Jorgensen, W. L., Chandrasekhar, J., Madura, J. D., Impey, R. W. & Klein, M. L. Comparison of simple potential functions for simulating liquid water. *J. Chem. Phys.* **79**, 926–935 (1983).
51. Evans, D. J. & Holian, B. L. The Nose-Hoover thermostat. *J. Chem. Phys.* **83**, 4069–4074 (1985).
52. Saito, H., Nagao, H., Nishikawa, K. & Kinugawa, K. Molecular collective dynamics in solid para-hydrogen and ortho-deuterium: The Parrinello-Rahman-type path integral centroid molecular dynamics approach. *J. Chem. Phys.* **119**, 953–963 (2003).
53. Hess, B., Bekker, H., Berendsen, H. J. C. & Fraaije, J. G. E. M. LINCS: a linear constraint solver for molecular simulations. *J. Comput. Chem.* **18**, 1463–1472 (1997).
54. Piche, S. W. Steepest descent algorithms for neural network controllers and filters. *IEEE Trans. Neural Netw.* **5**, 198–212 (1994).
55. Humphrey, W., Dalke, A. & Schulten, K. VMD: visual molecular dynamics. *J. Mol. Graph.* **14**, 33–38 (1996).
56. Mendels, D., Piccini, G. & Parrinello, M. Collective variables from local fluctuations. *J. Phys. Chem. Lett.* **9**, 2776–2781 (2018).
57. Bonomi, M. et al. PLUMED: a portable plugin for free-energy calculations with molecular dynamics. *Comput. Phys. Commun.* **180**, 1961–1972 (2009).
58. Kutzner, C. et al. More bang for your buck: improved use of GPU nodes for GROMACS 2018. *J. Comput. Chem.* **40**, 2418–2431 (2019).

## AUTHOR CONTRIBUTIONS

A.G.: devised the computational protocol and prepared the model systems, performed all calculations, analyzed the data, writing—software, and wrote and edited the original and the revised manuscript. H.R.: supervision, reviewing—editing, and edited the original and the revised version of the manuscript. S.P.: reviewing—editing and edited the original and the revised version of the manuscript. F.F.: reviewing—editing and edited the original and the revised version of the manuscript.

## COMPETING INTERESTS

The authors declare no competing interests.

## ADDITIONAL INFORMATION

**Supplementary information** The online version contains supplementary material available at <https://doi.org/10.1038/s41545-022-00173-2>.

**Correspondence** and requests for materials should be addressed to Heidar Raissi.

**Reprints and permission information** is available at <http://www.nature.com/reprints>

**Publisher's note** Springer Nature remains neutral with regard to jurisdictional claims in published maps and institutional affiliations.



**Open Access** This article is licensed under a Creative Commons Attribution 4.0 International License, which permits use, sharing, adaptation, distribution and reproduction in any medium or format, as long as you give appropriate credit to the original author(s) and the source, provide a link to the Creative Commons license, and indicate if changes were made. The images or other third party material in this article are included in the article's Creative Commons license, unless indicated otherwise in a credit line to the material. If material is not included in the article's Creative Commons license and your intended use is not permitted by statutory regulation or exceeds the permitted use, you will need to obtain permission directly from the copyright holder. To view a copy of this license, visit <http://creativecommons.org/licenses/by/4.0/>.

© The Author(s) 2022